Available online at www.sciencedirect.com
SCIENCE DIRECT®
Earth and Planetary Science Letters 233 (2005) 213–228
EPSL
www.elsevier.com/locate/epsl

Effect of mineral phase transitions on sedimentary basin subsidence and uplift

Boris J.P. Kaus[a,*], James A.D. Connolly[a], Yuri Y. Podladchikov[b], Stefan M. Schmalholz[b]

[a]*Earth Sciences Department, ETH Zürich, Sonneggstrasse 5, CH-8092 Zürich, Switzerland*
[b]*Physics of Geological Processes, University of Oslo, P.O.Box 1048 Blindern, Oslo, Norway*

Received 22 April 2004; received in revised form 18 August 2004; accepted 14 January 2005
Available online 19 March 2005
Editor: B. Wood

Abstract

Metamorphic phase transitions influence rock density, which is a major parameter affecting lithosphere dynamics and basin subsidence. To assess the importance of these effects, we have computed realistic density models for a range of crustal and mantle mineralogies from thermodynamic data by free-energy minimization. These density distributions are incorporated into one- and two-dimensional kinematic models of basin subsidence. The results demonstrate that, compared to models in which density is solely temperature dependent, phase transitions have the effect of increasing post-rift subsidence while decreasing syn-rift subsidence. Discrepancies between our model results and those obtained with the conventional uniform stretching models can be up to 95% for reasonable parameter choices. The models also predict up to 1 km of syn-rift uplift as a consequence of phase transitions. Mantle phase transitions, in particular the spinel–garnet–plagioclase–lherzolite transitions are responsible for the most significant effects on subsidence. Differences in mantle composition are shown to be a second-order effect. Parameterized density models are derived for crustal and mantle rocks, which reproduce the main effects of the phase transitions on subsidence.

Keywords: sedimentary basins; subsidence; mineral phase transitions; uplift

1. Introduction

One of the most widely used models for subsidence of sedimentary basins formed by extension is the uniform stretching model (USM), which assumes that subsidence is caused by crustal thinning and by thermal cooling [1]. An important feature of the USM formulation is that lithospheric density is assumed to depend only on temperature, a model we designate as the temperature-dependent density (TDD) formulation. The TDD formulation has been applied successfully in many situations, but it cannot

* Corresponding author. Now at: USC, 3651 Trousdale Pkwy., Los Angeles, CA 90089-0740, USA. Tel.: +1 213 821 3903.
E-mail address: bkaus@usc.edu (B.J.P. Kaus).

0012-821X/$ - see front matter © 2005 Elsevier B.V. All rights reserved.
doi:10.1016/j.epsl.2005.01.032

explain certain common observations (e.g., [2], and references therein). The most prominent difficulty is that many basins have relatively thin syn-rift sediments, but thick post-rift sediments [3–7]. To explain the thickness of the post-rift sediments with the TDD formulation, extensive stretching is required; this is at odds with the small thickness of syn-rift sediments. The widespread phenomenon of basin uplift during overall extension of the lithosphere (e.g., in the Vøring Basin; see [8]) creates a second difficulty for the TDD formulation. A thin crust is required (<1/7 of the lithospheric thickness) to explain this phenomenon. Such crustal thicknesses contradict geophysical observations suggesting crustal thickness is typically 30–40 km. Uplift usually occurs preceding rifting or after a finite amount of extension. An additional problem with the TDD formulation is posed by the fact that many basins have a phase of accelerated subsidence rates during the post-rift thermal subsidence phase [9,10]. The TDD formulation predicts that the subsidence rate decreases with time t as $t^{-0.5}$, and thus this can only be explained with non-thermal mechanisms [10–12]. To rectify these problems refinements of the TDD formulation have been proposed that include depth-dependent stretching [4,5], active rifting [13], interaction between lithospheric rheology and erosion [14] or mineral phase transitions (e.g., [11,15–17]. Here we focus on a refinement of this model in which lithospheric density is adjusted to account for phase transitions that occur in response to the geodynamic cycle.

Most of the models that have been proposed to explain shortcomings of the TDD formulation involve complexity or rely on parameters such as the lithospheric rheology, which are poorly constrained. However, the conditions and consequences of the metamorphic phase transitions that occur during lithospheric thinning are constrained from field observations, experimental studies and thermodynamic theory. We exploit the latter to construct a realistic lithospheric density model and to assess its consequences for basin subsidence.

That metamorphic phase transitions influence basin subsidence has been recognized for several decades. It has been suggested in [18] and [19] that crustal phase transitions around the Moho could affect uplift and subsidence. Numerical and analytical studies that concentrated on phase transitions in crustal rocks [9,10,12,17,20,21], in mantle rocks [11,15], or in both [22] demonstrated that phase transitions cause syn-rift uplift preceding rifting, greater post-rift subsidence then in the TDD formulation and periods of accelerated subsidence. Lobkovsky and coworkers [23,24] proposed a model in which partial melt, emplaced and solidified in lenses below the rift center, is transformed into eclogite causing accelerated post-rift subsidence. Their model requires a nearly impermeable Moho and predicts that eclogite lenses remain present after the completion of extension, which may be seismically detectable.

The applicability of most of the models described above is limited, since they typically only consider a single discontinuous phase transition. Natural rocks have continuous reactions. Many of these reactions have only small density effects, but the cumulative effect of these reactions can be significant. The optimal approach is to consider all the reactions that may occur in the lithosphere. Such an analysis in combination with basin subsidence was done by Petrini et al. [22], who used a realistic density distribution for both mantle and crustal rocks and demonstrated that phase changes lead to more post-rift subsidence and less syn-rift subsidence. However, they restricted their analysis to small stretching factors (δ=1.5) and did not detect syn-rift uplift as observed in [11] and [15].

Here we follow the same approach by coupling realistic density distributions with a kinematic subsidence model. To estimate the sensitivity of the results to the chemical composition of the lithosphere, we compute density models for a range of different mantle and crustal compositions. The results are then compared with the TDD formulation and parameterized density maps are derived that reproduce results of 'real' density maps up to reasonable accuracy and thus yield additional insight into the way phase transitions influence subsidence.

2. Representative phase diagrams and density distributions for crustal and upper mantle rocks

Phase assemblages at the pressure (P) and temperature (T) conditions of interest were computed using

Table 1
Chemical crustal and mantle compositions considered in this work

	Hawaiian pyrolite[a]	MOR-harzburgite pyrolite[b]	Depleted (Tinaquillo) pyrolite[a]	Total crust[c]	Granodiorite[d]
SiO_2	45.2	45	45	57.3	66.1
TiO_2	0.71	0.17	0.1	0.9	0.54
Al_2O_3	3.54	4.4	3.2	15.9	15.7
Fe0	8.47	7.6	7.7	9.1	4.4
MgO	37.5	38.8	40	5.3	1.74
CaO	3.08	3.4	3	7.4	1.5
Na_20	0.57	0.4	0.2	3.1	3.75
MnO	0	0.11	0	0	0
K_20	0	0	0	1.1	2.78
H_20	0	0	0	Saturated	Saturated

[a] [35].
[b] [58].
[c] [27].
[d] [28].

Table 2
Mineral solution notation, formulas and model sources (1—[30]; 2—[53]; 3—[54]; 4—[55]; 5—[31]; 6—[56])

Symbol phase		Formula	Reference
Amp	Amphibole	$Ca_{2-2w}Na_{2w}Mg_xFe_{(3+2y+z)(1-x)}Al_{3-3y-w}Si_{7+w+y}O_{22}(OH)_2$	1
Bt	Biotite	$KMg_{(3-y)x}Fe_{(3-y)(1-x)}A1_{1+2y}Si_{3-y}O_{10}(OH)_2$	1
Car	Carpholite	$Mg_xFe_{(1-x)}Al_2Si_2O_6(OH)_2$	Ideal
Chl	Chlorite	$Mg_{(5-y+z)x}Fe_{(5-y+z)(1-x)}Al_{2(1+y-z)}Si_{3-y+z}O_{10}(OH)_8$	2
Cpx	Clino-pyroxene	$Na_{1-y}Ca_yMg_{xy}Fe_{(1-x)y}Al_ySi_2O_6$	6
Crd	Cordierite	$Mg_{2x}Fe_yMn_{(1-x-y)}Al_2SiO_5(OH)_2$	Ideal
crn	Corundum	$A1_20_3$	1
Ctd	Chloritoid	$Mg_xFe_yMn_{(1xy)}Al_2SiO_5(OH)_2$	1
Grt	Garnet	$Fe_{3x}Ca_{3y}Mn_{(1-x-y)}A1_2Si_3O_{12}$	1
ilm	Ilmenite	$FeTiO_3$	1
Ilm	Ilmenite	$Mg_xMn_yFe_{1-x-y}TiO_3$	Ideal
Kfs	Alkali feldspar	$Na_xK_yAlSi_3O_8$	3
lws	Lawsonite	$CaAl_2Si_2O_7(OH)_2 \cdot (H_2O)$	1
lmt	Laumontite	$CaAl_2Si_4O_{12} \cdot (4H_2O)$	1
Ol	Olivine	$Mg_xFe_{1-x}SiO_4$	1
Opx	Ortho-pyroxene	$Ca_zMg_{x(2-y)(1-z)}Fe_{(1-x)(2-y)(1-z)}Al_{2y}Si_{2-y}O_6$	1
Pl	Plagioclase	$Na_xCa_{1-x}Al_{2-x}Si_{2+x}O_8$	4
Phg	Phengite	$K_xNa_{1-x}Mg_yFe_zAl_{3-2(y+z)}Si_{3+y+z}O_{10}(OH)_2$	1
Melt	Melt	Na–Mg–Al–Si–K–Ca–Fe hydrous silicate melt	5
prh	Prehnite	$Ca_2Al_2Si_3O_{10}(OH)_2$	1
pmp	Pumpellyite	$Ca_4MgAl_5Si_6O_{21}(OH)_7$	1
qtz	Quartz	SiO_2	1
rt	Rutile	TiO_2	1
Sa	Sanidine	$Na_xK_yAlSi_3O_8$	1
Spl	Spine1	$Mg_xFe_{1-x}AlO_3$	1
sph	Sphene	$CaTiSiO_5$	1
St	Staurolite	$Mg_{4x}Fe_{4y}Mn_{4(1xy)}Al_{18}Si_{7.5}O_{48}H_4$	1
zo	Zoisite	$Ca_2Al_3Si_3O_{12}(OH)$	1

The compositional variables w, x, y, and z may vary between zero and unity and are determined as a function of pressure and temperature by free-energy minimization.

free-energy minimization [25,26]. The minimization program requires thermodynamic data for end-member phase compositions together with solution models to compute relative proportions, compositions and densities of the stable mineralogy.

The bulk compositions considered here are listed in Table 1. Taylor and McLennan [27] proposed a model for the continental crust consisting of 75% Archean crust and 25% andesitic crust, to represent the different Archean and post-Archean crustal growth processes. A second crustal model assumes the crust to have a granodioritic composition [28]. Three different mantle models have been employed. These are variations of the pyrolite model originally proposed by Ringwood [29] and represents the mean chemical composition of the upper mantle. The compositions that are used for calculations range from an incompatible-element-enriched mantle (Hawaiian Pyrolite) to a normal upper mantle (MOR-pyrolite), to a depleted mantle (Tinaquillo lherzolite). The crust is assumed to be saturated in water, whereas the mantle is anhydrous. Melting in the crust is not taken into account.

The model bulk rock compositions were simplified to include the oxides SiO_2, TiO_2, $A1_2O_3$, FeO, MgO, CaO, Na_2O and MnO. Cr_2O_3 is not available in the database of Holland and Powell [30] and was therefore not considered. Chromium would effect the spinel-stability field, but due to its low volumetric content (<0.5%) its overall contribution to the mean bulk density is minor. The same reasoning justifies neglecting other minor components such as P_2O_5 and K_2O. The thermodynamic mineral database of Holland and Powell [30] was used in the calculations, together with solution models as listed in Table 2.

The accuracy of the solution models was specified to resolve compositions with a maximum error of 2 mol%. Melting of mantle rocks is accounted for by the pMELTS model [31]. Solution models compiled by Holland and Powell were used for crystalline solution phase. To test the effect of using solution models from

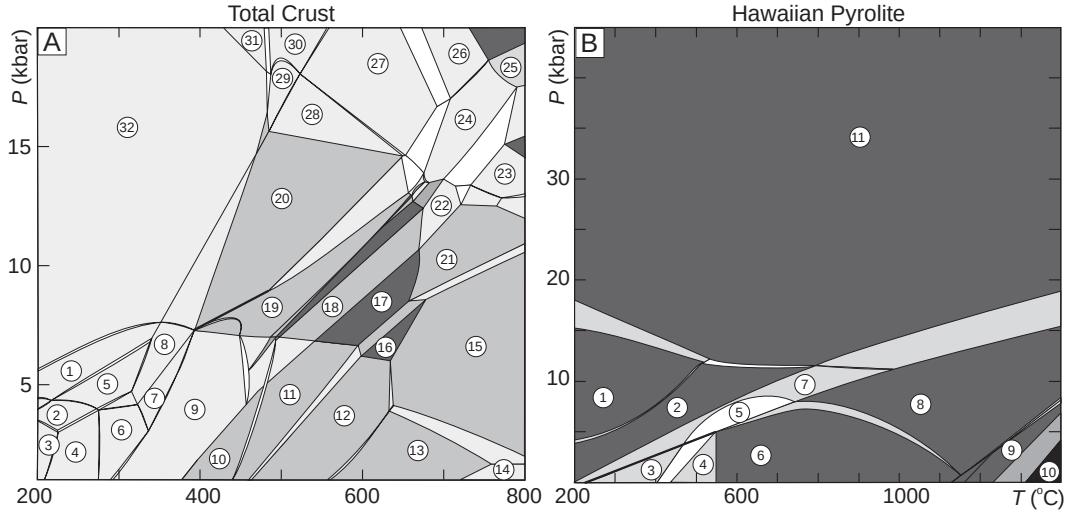

Fig. 1. Phase diagram section of lithospheric rocks with (A) a 'total crust' chemical bulk composition (see Table 1). Numbers correspond to the phase assemblages (see Table 2 for abbreviations): 1—Chl+Phg+lws+sph, 2—Chl+Kfs+pmp+sph, 3—Chl+Kfs+sph+lmt, 4—Chl+Kfs+sph+prh, 5—Chl+Phg+pmp+sph, 6—Chl+Kfs+sph+lmt, 7—Bt+Chl+zo+sph, 8—Chl+Phg+zo+sph, 9—Bt+Chl+zo+sph, 10—Bt+Chl+sph, 11—Bt+Chl+rt, 12—Bt+Chl+ilm, 13—Bt+Crd+ilm, 14—Bt+Crd+fa+ilm, 15—Bt+Grt+ilm, 16—Bt+Amp+ilm, 17—Bio+rt, 18—Bt+Phg+rt, 19—Phg+zo+sph, 20—Phg+zo+sph, 21—Bt+Grt+rt, 22—Bt+Phg+Grt+rt, 23—Bt+Grt+rt, 24—Phg−Grt−rt, 25—Phg+Grt+rt, 26—Phg+Pa+Grt+rt, 27—Phg+Grt+zo+rt, 28—Phg+Grt+zo+sph+rt, 29—Phg+Grt+law+sph, 30—Phg+Grt+lws+rt, 31—Chl+Phg+lws+rt. 32—Chl+Phg+lws+sph. Phases 1–27, 29–31 contain qtz, phases 1–8, 20, 23–32 contain Cpx, phases 9–24, 26–32 contain Amp and phases 1–19, 21–25 contain P1. (B) A 'Hawaiian Pyrolite' mantle composition. Numbers refer to the phase relationships: 1—Cpx+Opx+Ol+Ilm+crn, 2—Cpx+Opx+Ol+Spl+Ilm, 3—Cpx+Opx+$P1_1$+$P1_2$+Ol+Ilm, 4—Cpx+Opx+$P1_1$+$P1_2$+Ol+rt, 5—Cpx+Opx+$P1_1$+Ol+Spl+Ilm+rt, 6—Cpx+Opx+Pl+Ol+rt, 7—Cpx+Opx+Ol+Spl+Ilm+P1, 8—Cpx+Opx+Pl+Ol+Ilm, 9—Cpx+melt+Pl_2+O1+Ilm, 10—melt+Ol+Ilm, 11—Cpx+Opx+Ol+Ilm+Grt.

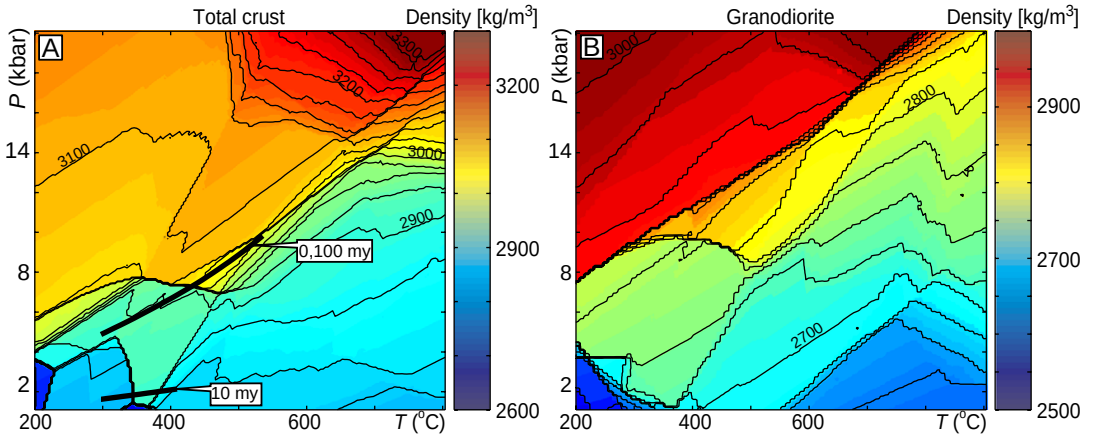

Fig. 2. Density as a function of pressure and temperature for different crustal rocks, with a bulk chemical composition given in Table 1. Superposed lines in panel (A) shows the P–T distribution in a lithosphere with parameters of Fig. 5 and δ=6 (see Section 4 of the text).

other sources, calculations were done with a range of different solution models, and it was found that the effect on the density structure was relatively minor. Furthermore, some of the computations of Sobolev and Babeyko [32]) who used independently developed software and databases have been redone here. These computations showed good agreement, both for the density structure and for the phase diagram section topology, which gives additional confidence in the robustness of our approach.

The most important mantle phase transitions are the spinel–lherzolite to garnet–lherzolite transition that occurs around at pressures from 12 to 20 kbar and the plagioclase–lherzolite to spinel/garnet–lherzolite that occurs at lower pressures (Fig. 1). These results are in agreement with previous computational results and experimental data (see, e.g., [33,34]). Partial melting of mantle rocks commences at temperatures above 1200 °C, which is in agreement with experimental data [35].

The corresponding densities for these two compositions as well as for the other three compositions listed in Table 1 are shown in Figs. 2 and 3. The most significant density change in the crust is the eclogite (plagioclase-out) transition (Fig. 1). The ‘total-crust’

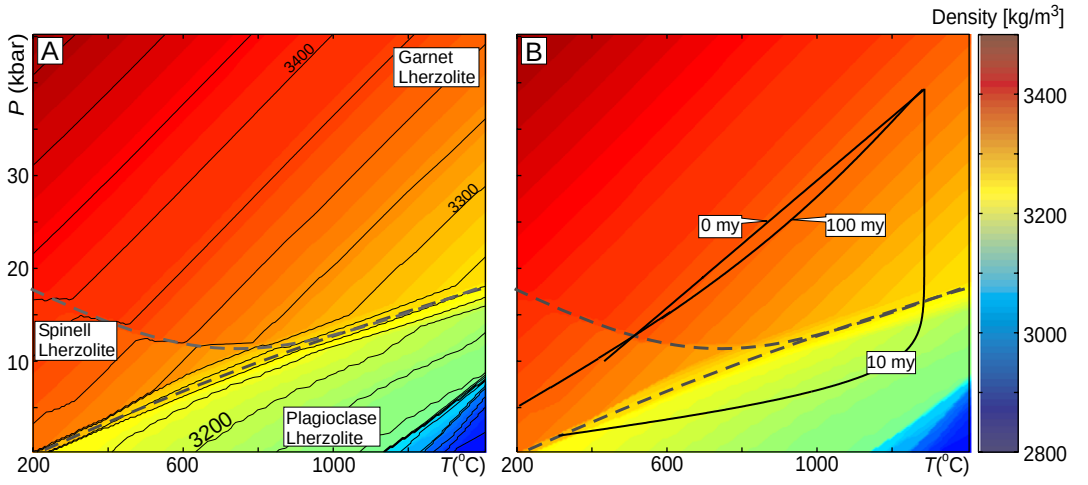

Fig. 3. Density as a function of pressure and temperature for a Hawaiian Pyrolite mantle composition with a bulk chemical composition given in Table 1. Superposed lines in panel (B) shows the P–T distribution in a lithosphere with parameters of Fig. 5 and δ=6 (see Section 4 of the text).

density distribution has densities that are slightly higher then the 'granodioritic' crustal composition. Mantle densities are discontinuous across the stability fields for garnet–, spinel–, and plagioclase–lherzolite, and at the onset of melting. The density change related to the spinel–garnet phase transition is around 30–40 kg/m^3. This is the only phase transition that was considered in [11] and [15]. However, the density change that is related to the transformation of spinel–lherzolite to plagioclase–lherzolite (80–100 kg/m^3) is larger than the density effect of the spinel–garnet transition. Therefore, the plagioclase-in transition could potentially cause additional post-rift subsidence and syn-rift uplift.

3. One-dimensional subsidence model

The influence of phase transitions on sedimentary basin subsidence was studied with a one-dimensional kinematic model. The lithosphere is assumed to consist of a crust and a mantle. During a rifting period of duration t_{rift}, the lithosphere is uniformly thinned in such a way that the ratio between the post-rift and the pre-rift thickness is

$$\delta = \frac{H_{\text{lith}}^{\text{pre}}}{H_{\text{lith}}^{\text{post}}} \tag{1}$$

here $H_{\text{lith}}^{\text{pre}}$ is the pre-rift and $H_{\text{lith}}^{\text{pos}}$ the post-rift lithospheric thickness. During and after rifting, perfect isostasy is assumed, i.e., the pressure or lithostatic load at depth $H_{\text{lith}}^{\text{pre}}$ is constant. The subsiding basin is filled with sediments of constant density (2200 kg/m^3), and thinning of the lithosphere is compensated by up-welling of mantle asthenosphere. Thinning of the lithosphere occurs incrementally between time steps to include effects of sediment blanketing and thermal cooling during rifting. Sediments are also thinned incrementally to conserve volume of the already deposited sediments. The effects of erosion are not incorporated and sediments can be uplifted above the original zero level.

The thermal evolution during and after rifting is computed with:

$$\rho c_{\text{p}}\left(\frac{\partial T}{\partial t} + v_{\text{z}}\frac{\partial T}{\partial z}\right) = \frac{\partial}{\partial z}\left(k\frac{\partial T}{\partial z}\right) + \text{A} \tag{2}$$

where ρ is density, c_{p} heat capacity, t time, z vertical coordinate, v_{z} vertical velocity during thinning, T temperature, k thermal conductivity and A radioactive heat production. Radioactive elements are assumed to be only present in the crust. The boundary conditions are constant temperature of T=0 °C on top of the model and a constant temperature of T=T_{base}, at the base of the model. The initial condition is a steady-state temperature distribution. Density is computed with three approaches. The first approach is the classic approach in which density is temperature-dependent through the thermal expansivity α. The second approach takes the pressure dependence of density into account, which yields the following density–pressure–temperature relationship

$$\rho = \rho_0(1 - \alpha T + \beta P). \tag{3}$$

The third approach takes density from our computed density maps (Figs. 2 and 3). At lower temperatures, metamorphic reactions proceed slowly and metastable phase assemblages can occur (e.g., [36]) so that our assumption of equilibrium phase assemblages may not be valid. Therefore, we assume that the density structure at temperature lower than 200 °C, is the same as that at 200 °C. Simulations in which this equilibrium temperature was increased to 300 °C did not show a significant difference. An additional effect that has been ignored in the current study is the effect of latent heat. This effect was considered by [15], who demonstrated that it causes maximum changes in temperature of around 10 °C, which is insignificant on a lithospheric scale (e.g., [37]).

Eq. (2) is solved numerically with an implicit finite-difference scheme for the diffusion terms [38] and temperature advection is calculated using the method of characteristics. The numerical code was benchmarked versus variable analytical solutions for diffusion and advection problems, versus the analytical solution of [1] and versus results of a numerical basin code independently developed by one of the co-authors (SMS). The nonlinearity in the problem, which is introduced through the dependency of density on temperature and pressure, in combination with isostatic equilibrium, is solved iteratively. For the calculations of density changes conservation of volume is assumed. Each one-dimensional element between two grid points is assigned a density and the

size of this element does not change during the iterative density calculations. An alternative approach is to conserve mass so that the product of element length times its density is the same before and after the density changes. The numerical resolution was 200 grid points in vertical direction. Resolution tests have been performed to ensure that the temporal and spatial resolution is sufficient.

4. Results

4.1. Basin subsidence with and without phase transitions

A range of calculations have been performed for the solely temperature-dependent density (TDD) formulation, a model in which density is solely dependent on P and T (Eq. (3)), and a model in which 'realistic' densities are taken from thermodynamic calculations (Fig. 4). Differences between the TDD formulation and the density formulation of Eq. (3) are insignificant, indicating that the term, βP in Eq. (3) can be neglected. However, the incorporation of realistic densities does have a large influence on the subsidence behavior. In general, syn-rift subsidence is decreased and post-rift subsidence is increased. During the syn-rift phase, most models are initially close to the subsidence behavior of TDD model. After ~5 million years, deviations can be observed, which in some cases result in an uplift of several hundred meters. After rifting ceases, models with realistic densities give significantly more post-rift subsidence compared to TDD formulations. Moreover, realistic density models lead to episodes of both increased and decreased subsidence rate relative to TDD models.

Syn-rift subsidence in the TDD formulation is dependent on the density contrast between mantle and crust in such a way that a lower mean crustal density results in more syn-rift subsidence (for the same average density of the infilled sediments). An

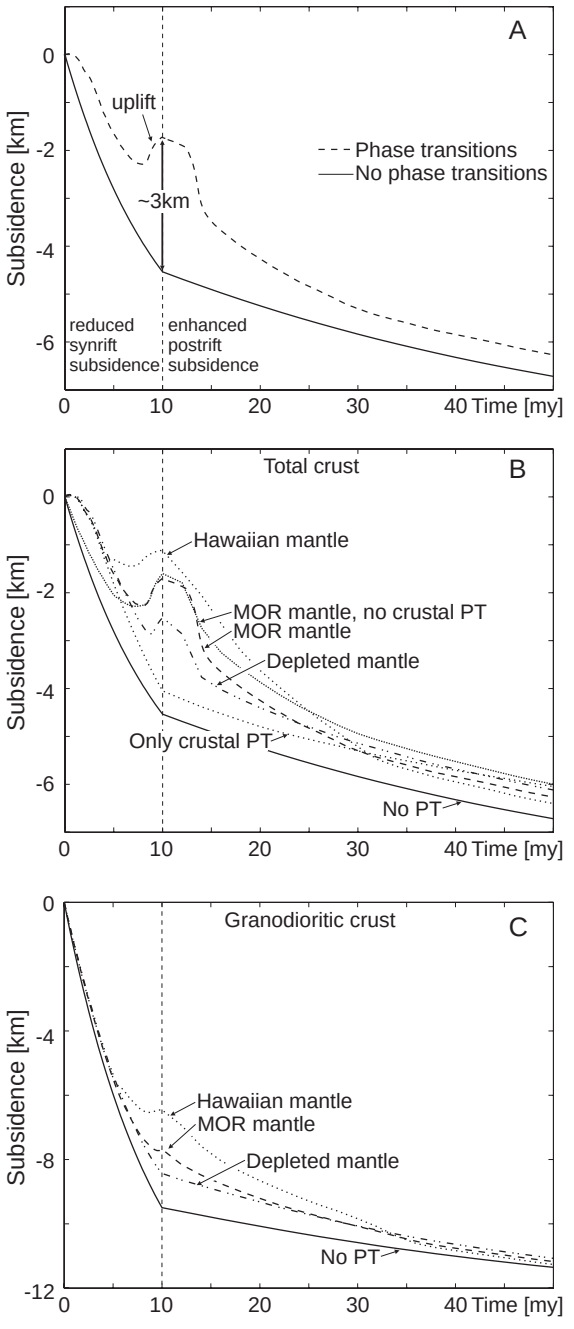

Fig. 4. Effect of phase transitions on basin subsidence for a model with δ=3, H^{pre}_{crust}=35 km, H^{pre}_{mantle}=90 km and T_{base}=1300 °C. (A) Comparison of a model with phase transitions and a model without phase transitions. The model with phase transitions has a 'total-crust' crustal density and a MOR mantle density. The model without phase transitions has been computed with ρ^c_0=2900 kgm^{-3}. (B) The effect of mantle compositions on subsidence for 'total crust' crustal model. The model with crustal phase transitions deactivated assumes ρ^c_0=2995 kgm^{-3}. (C) The effect of mantle compositions on subsidence for 'granodioritic' crustal model. ρ^c_0=2730 kgm^{-3}.

identical effect can be observed here in models with a realistic crustal density (Fig. 4). Models with a 'granodioritic' density subside more during the syn-rift phase than models with a 'total-crust' density. This reflects the fact that the 'total-crust' model is largely based on inferred Archean crustal compositions that are denser than granodioritic compositions.

Post-rift subsidence in the TDD formulation is independent of the density contrast between crust and mantle. Thus the large differences that are observed during the post-rifting phase in all models with realistic densities (Fig. 4C) are entirely due to the effect of phase transitions. Depending on the mineralogy, the additional post-rift subsidence ranges from ~30% to 100%.

To establish whether this additional subsidence is caused by mantle or by crustal phase transitions, two experiments were performed: one in which the crustal phase transitions and one in which the mantle phase transitions have been deactivated. Deactivating phase transitions has been done by replacing the realistic density model by a TDD formulation (Eq. (3) with β=0). The results demonstrate that mantle phase transitions are, to a large extent, responsible for the additional post-rift subsidence that is observed (Fig. 4B).

Syn-rift uplift is observed in almost all models with realistic densities (Fig. 4), and occurs either at the onset of rifting or after a finite amount of thinning. The amount of syn-rift uplift at the onset of rifting is relatively small (maximum $\approx$50 m) compared to the amount of uplift that is obtained after a finite amount of extension. However, it has an impact on the total amount of syn-rift subsidence, since it prevents the basin from subsiding for ~1 million years. In the next section, we analyze the reasons for the syn-rift uplift and study its dependence on various parameters.

4.2. Effect of stretching factor on basin subsidence

Increasing the stretching factor 6 with a realistic density model (Fig. 5) enhances the effect of phase transitions in that it results in less syn-rift subsidence and more post-rift subsidence than in simple density models. For example, a stretching factor of δ=1.5 causes additional post-rift subsidence of 20%–40%, whereas stretching factors of δ=4 and δ=6 cause additional subsidence of 50%–110%, depending on the composition of crustal and mantle. Up to 1000 m of syn-rift uplift is observed in models with a 'total-crust' crustal composition combined with either a Hawaiian—or a MOR-pyrolitic mantle composition for stretching factors of 4 and 6. If syn-rift uplift occurs, it is followed by a period of increased post-rift subsidence.

The phenomena that cause syn-rift uplift and extensive post-rift subsidence in the simulations with realistic density models can be understood by considering the variations in density caused by phase transformations during and after rifting (Figs. 2A and 3B). At the onset of rifting, the mantle lithosphere is composed of spinel–lherzolite up to a pressure of 12 kbar (corresponding to a depth of 41 km) and of garnet–lherzolite at greater pressures. During rifting, spinel–lherzolite and part of the garnet–lherzolite transforms into plagioclase–lherzolite. The onset of syn-rift uplift (Fig. 5) corresponds to the introduction of plagioclase–lherzolite into the model mantle and the end of syn-rift uplift, at ~ 8 myr, corresponds to the complete transformation of spinel–lherzolite into plagioclase–lherzolite. After rifting ceased, the mantle cools and plagioclase–lherzolite transforms back into garnet– and spinel–lherzolite. Simulations with lower stretching factors (e.g., δ=1.5) do not result in the formation of plagioclase–lherzolite and have no syn-rift uplift (see Fig. 5). Thus the formation of plagioclase lherzolite is an influential reaction for basin subsidence.

Syn-rift uplift has a different magnitude for different mantle compositions. A depleted mantle composition leads to generally less syn-rift uplift (Fig. 5). This can be attributed to the fact that a depleted mantle has a higher Mg-content, which favours the growth of olivine and orthopyroxene, and increases the density of the plagioclase–lherzolite by 10–25 kg/m^3. This effect shows that syn-rift uplift is dependent on the mantle composition. The post-rift and total subsidence, however, are only weakly dependent on the mantle composition (Fig. 5). We thus conclude that syn-rift uplift is a consequence of the generally lower density of the plagioclase–lherzolite compared to that of spinel– and garnet–lherzolite, and that this uplift will only occur if the stretching factor δ exceeds a minimum value δ_{crit} (Fig. 5).

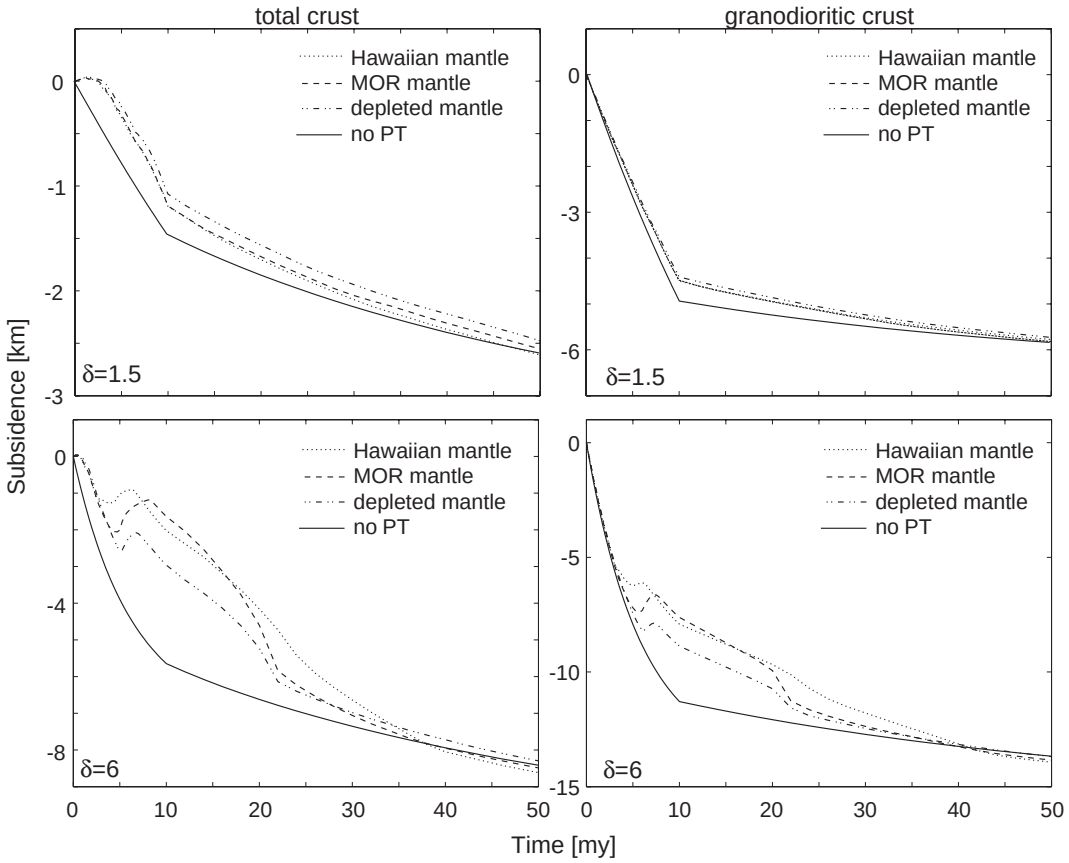

Fig. 5. Effect of stretching factor δ on basin subsidence for different mantle and crustal compositions. ρ_c^0 in models without phase transitions is chosen to match the long-term total subsidence.

4.3. Parameterized density models

Our simulations with realistic density models indicate that the garnet–spinel–plagioclase–lherzolite transitions have the greatest influence on basin subsidence. The simulations also demonstrate that crustal phase transitions do not have a large impact on post-rift subsidence, but that the crustal rock assemblage does influence the syn-rift subsidence since it changes the *mean* density of the crust. The effect of the crustal density model is thus similar to a TDD formulation with a crustal density chosen to correspond to the mean density (Table 3).

To verify whether the mantle transitions are indeed the most important ones, and to reduce the computed density maps to a simple parameterization, the computed 'real' density distributions have been fit by least-squares (see Appendix A). Partial melting has not been included in the current density parameterization since the melt is assumed to be rapidly removed by dikes [39] or a porous flow mechanism [40] which changes the bulk chemistry of the rocks and invalidates the model used here.

The 'real' density models are compared with the parameterized density models for different stretching

Table 3
Model parameters

Symbol	Meaning	Value
k	Thermal conductivity	3 $Wm^{-1}K^{-1}$
A	Radioactive heat production	10^{-6} Wm^{-1}
c_p	Specific heat	10^3 $Jkg^{-1}K^{-1}$
α	Thermal expansivity	3×10^{-5} K^{-1}
β	Compressibility	1×10^{-11} Pa^{-1}

factors, compositions and crustal/mantle thicknesses (Fig. 6). The maximum error in total, syn-rift and post-rift subsidence between the real models and the parameterized models is around 10%. The parameterized models reproduce the most important features of the real models, including syn-rift uplift and accelerated post-rift subsidence. The low density of plagioclase–lherzolite compared to spinel/garnet–lherzolite is responsible for syn-rift uplift and a subsequent phase of accelerated post-rift subsidence (Fig. 6). Increasing the density of plagioclase–lherzolite reduces uplift. The total subsidence after post-rift subsidence remains unaltered.

4.4. Deviations from the TDD pure-shear stretching model

In this section, the parameterized density models are used to estimate the maximum syn-rift uplift and post-rift subsidence that can be produced by phase transition models. The *maximum* effect of phase transitions in the models presented before was obtained for a combination of a 'total-crust' crust and a MOR-pyrolite mantle. The *minimum* effects occurred for a granodioritic crust and a depleted-pyrolite mantle. An estimate of the deviations that phase transitions give with respect to TDD formulation are thus be made by performing systematic computations with both the minimum and the maximum model.

Several thousand computations have been performed, in which the stretching factor and the crustal thickness were varied, but the total lithospheric thickness and the base temperature were maintained constant (Fig. 7). Models with $H_{crust}/H_{lithos}<0.2$ are characterized by a phase of uplift at the beginning of the rifting period, as predicted by previous work [11]. This is followed by a phase of subsidence and, in some cases, by an additional uplifting phase (Fig. 7A). Maximum obtainable syn-rift uplift ranges from 700 m in the minimum model to ~1000 m in the maximum model.

Decreasing T_{base} to 1000 °C decreases the maximum syn-rift uplift by 30%. In addition, the critical stretching factor to initiate syn-rift uplift is increased from 2–2.5 to 3–3.5. Increasing T_{base} to 1400 °C decreases the critical stretching factor from ~2 to 1.5. Increasing the total lithospheric thickness from 110 km to 160 km increases the critical stretching factor required to initiate syn-rift uplift from 2 to 3, and narrows the range of H_{crust}/H_{lithos} for which syn-rift uplift occurs. If lithospheric thickness is decreased, the H_{crust}/H_{lithos}-range widens from 0.15 to 0.4 but the maximum uplift is decreased by ~20%.

Compared to the TDD formulation, phase transitions cause additional post-rift subsidence of at least 20%, and as much as 90% in the maximum model or 50% in the minimum model (Fig. 7D). Increasing T_{base} to 1400 °C increases the subsidence

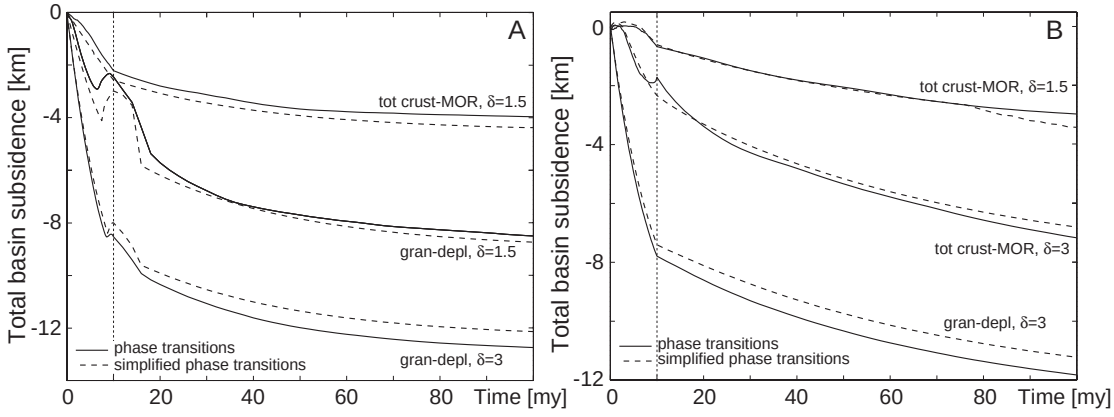

Fig. 6. Comparison of basin subsidence with real and simplified density models, for a stretching factor of δ=1.5 and δ=3, and for (A) a crustal thickness of 35 km and a mantle thickness of 70 km and (B) a crustal thickness of 35 and a mantle thickness of 110 km.

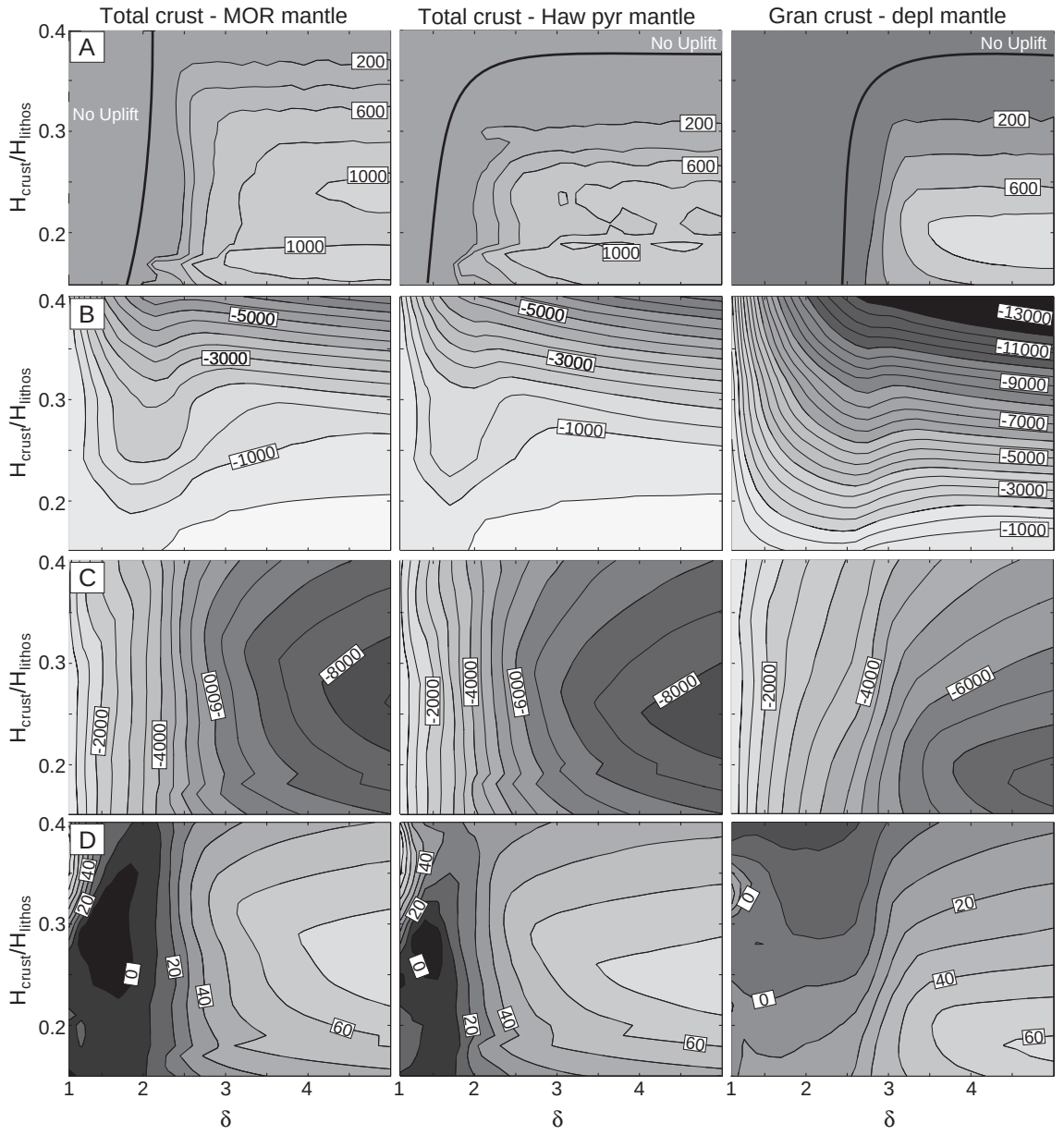

Fig. 7. (A) Contour plot of maximum syn-rift uplift at the end of the rifting phase as a function of stretching factor and crustal thickness normalized over the lithospheric thickness. The model on the left is with a density distribution ('MOR mantle' and 'total-crust') which gives the maximum uplift. The model on the right gives the minimum uplift. (B) Total syn-rift subsidence (after 10 myr of rifting). (C) Total thermal subsidence (after 300 myr) in meters. (D) Percentage of additional post-rift subsidence compared to TDD models in which the density distribution is solely temperature-dependent.

by 20%, whereas decreasing T_{base} to 1000 °C halves the difference. Increasing the lithospheric thickness to 160 km increases the maximum deviations of the TDD formulation by 30% and decreasing the thickness to 80 km, decreases the deviations by 30%.

5. Discussion and conclusions

Realistic density models (Appendix A) that are reproduced by simple parameterizations have been implemented in kinematic basin simulations. The simulations demonstrate that, in general, phase transitions reduce syn-rift subsidence and increase post-rift subsidence compared to the uniform stretching (TDD) model, in which density is solely temperature-dependent. The deviations in post-rift subsidence from the TDD model resulting from realistic density models vary from ~20% at low stretching factors to >90% at greater stretching factors. Differences in mineralogy may result in different amounts of subsidence, but all the cases considered generate trends that deviate significantly from that predicted by TDD models. In distinction from the TDD model that does not result in syn-rift uplift for reasonable parameters, use of realistic density model can explain up to 1 km of syn-rift uplift. In contrast to simpler modelling efforts to account for the effect of phase transitions (e.g., [15]), which predicted syn-rift uplift preceding rifting, we obtain uplift during stretching. This syn-rift uplift is caused by the formation of plagioclase–lherzolite from spinel– and garnet–lherzolite, which occurs during rifting (Fig. 8). During the thermal post-rift stage, plagioclase–lherzolite is transformed back into spinel– and garnet–lherzolite, thereby causing an additional amount of postrift subsidence. A two-dimensional simulation points out that plagioclase–lherzolite mainly forms below the center of the basin (Fig. 8). Thus syn-rift uplift is to expected in the center of the basin only. Plagioclase–lherzolite will only be detectable seismically during, or shortly after, an active extension phase.

In our simulations, we assumed that phase assemblages are always at equilibrium. This assumption may require explanation. In general, metamorphic reactions are influenced by deformation, presence of volatiles, temperature, etc. In crustal rocks, volatiles strongly enhance metamorphic reaction kinetics (e.g., [41,36]. If these volatiles are removed during prograde metamorphism, reaction rates drop and the prograde metamorphic assemblage are preserved [37,42]. For anhydrous mantle assemblages, thermal activation is the dominant factor. It has been argued that anhydrous metamorphic reactions occur at geologically short timescales for temperatures above 600 °C [43]. We demonstrate that the mantle reactions have the largest impact on basin subsidence. Typical mantle temperatures are above 600 °C (Fig. 3A), at these temperatures both homogeneous and heterogeneous equilibrium are likely.

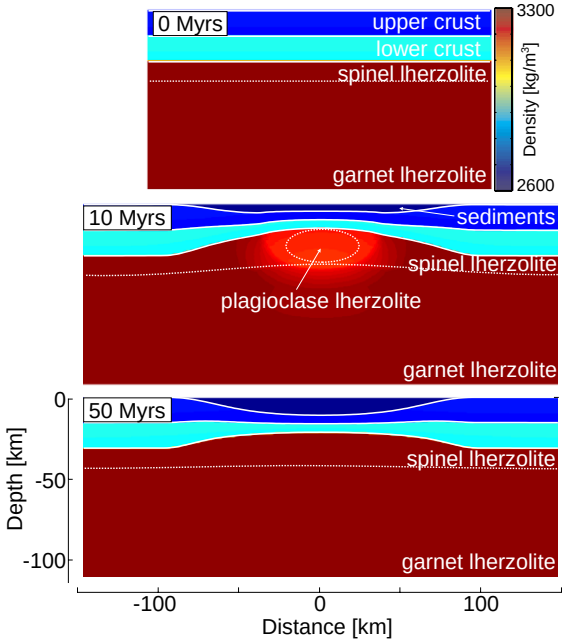

Fig. 8. Results of 2-D computations with phase transitions activated in the mantle only (MOR-model). The maximum stretching factor in the center of the basin is 3. The upper crust has a T-dependent density with ρ_0=2700 kgm^{-3} and the lower a T-dependent density with ρ_0=2900 kgm^{-3}. The initial crustal thickness is 35 km; stretching is active for 10 myr and the elastic thickness is 0 km. Plagioclase lherzolite appears in the mantle lithosphere during rifting but disappears after rifting has ceased. Modelling results have been obtained with TECMOD2D (http://www.geomodsol.com, [57]).

In all our models, the accommodation space created by subsidence is completely filled with sediments (i.e., water depth is zero). Once sediments are deposited, they will never be eroded. This implies that during phases of syn-rift uplift, sediments are uplifted above the initial zero level. We have performed additional simulations in which these sediments were eroded infinitely fast above the zero level. These simulations resulted in a factor two increase of the amount of syn-rift uplift. The total amount of subsidence, however, was nearly unaffected. Thus the simulations presented here can be

Table A1
The simplified crustal phase diagram is composed of two regions

Composition	Low-P region			High-P region		
	ρ_0	α $\times10^{-5}$	β $\times10^{-11}$	ρ_0	α $\times10^{-5}$	β $\times10^{-11}$
Total crust	2835	2.82	3.46	3060	1.96	1.34
Granodioritic	2683	8.57	4.85	2918	4.11	2.09

Density in each region can be computed with $\rho=\rho_0\ (1-\alpha T+\beta P)$, with P in Pascal (Pa) and T in degree Celsius (°C). The boundary between the two regions is given by $P=1.92\times10^6T-1.6\times10^7$ for the total crust and by $P=2\times10^6T-3.2\times10^8$ for a granodioritic crust.

regarded as being conservative with respect to the amounts of syn-rift uplift.

For more realistic two- and three-dimensional models, the effect of flexural isostasy has to be taken into account. A lithospheric flexural rigidity or effective elastic thickness [44,45] can decrease or damp the syn-rift uplift significantly only if the width of the area in which uplift occurs is considerably smaller than the flexural wavelength. Effective elastic thicknesses used for extensional basin modelling are usually small (smaller than around 5 km, e.g., [46,47]) providing flexural wavelengths smaller than around 100 km. Hence, for such values of effective elastic thickness, syn-rift uplift will be only slightly decreased for most basin and passive margin dimensions. The EET is frequently assumed to be a function of the depth of a particular isotherm ([44], and references therein). Syn-rift uplift occurs at the end of rifting, when isotherms are most elevated and the temperature-dependent EET is smallest. Thus phase transitions might have a considerable effect also in cases with large EETs. Furthermore, lateral heat conduction in two- and three-dimensional models will provide considerable different results only if the thinning factors vary strongly in the lateral direction causing strong lateral temperature variations (Fig. 8). Rheology may potentially influence our results in two ways: (1) the viscosity of the asthenosphere determines to a large extent how well the lithosphere is isostatically compensated. Large asthenospheric viscosities may reduce and delay the uplift phase. (2) Increasing the effective viscosity of the upper lithosphere will result in larger Deborah numbers and therefore larger effective elastic thicknesses. This may decrease syn-rift uplift as discussed above. However, more work in this direction is required to obtain insight in the interaction between phase transitions and rheologically controlled dynamical processes (see, e.g., [17]). In this paper, we have focussed on the effect of metamorphic reactions on basin subsidence by comparison with the simplest version of the stretching model. Subsequent modifications of this model such as depth-dependent stretching [4], depth of necking combined with flexural isostasy and erosion (e.g., [48,49]), ductile lower crustal flow [50], magmatic underplating and intraplate stresses can also cause additional subsidence and uplift in, e.g., the North Sea [51,52]. Most of these models have employed a simple TDD model. We have demonstrated here that the incorporation of more realistic density models may have a considerable effect in itself. Incorporating realistic densities in any of the

Table A2
The simplified mantle diagram is composed of three regions

$\rho=\rho_0(1-\alpha T+\beta P)$	Spinel lherzolite			Plagioclase lherzolite			Garnet lherzolite		
Pyrolite	ρ_0	α	β	ρ_0	α	β	ρ_0	α	β
Composition		$\times10^{-5}$	$\times10^{-11}$		$\times10^{-5}$	$\times10^{-11}$		$\times10^{-5}$	$\times10^{-11}$
Hawaiian	3369	3.87	9.54	3388	3.54	1.34	3270	3.67	1.65
MOR	3363	3.87	8.62	3387	3.54	1.34	3249	3.39	1.45
Depleted	3353	3.88	9.25	3371	3.56	1.34	3275	3.51	1.50

$P=\alpha T^2+bT+c$	Plagioclase–Spine1 boundary			Spinel–Garnet boundary		
Composition	a	$b\times10^6$	$c\times10^8$	a	$b\times10^6$	$c\times10^9$
Hawaiian	−345	1.96	−4.4	1825	−2.7	2.2
MOR	−460	1.99	−4.4	1946	−3.1	2.4
Depleted	−435	1.91	−4.1	1660	−2.9	2.4

Fitted functions for density in each region are indicated as well as the boundaries between the different regions.

models above will thus enhance the effects. Depth-dependent stretching caused by ductile crustal flow, for example, would, if combined with metamorphic reactions, require less differential stretching between crust and mantle lithosphere to obtain the same subsidence as depth-dependent stretching models without phase transitions. Phase transitions could in the same way enhance active rifting [13]) since it increases the buoyancy of the upwelling mantle dome. It seems unlikely that any of these mechanisms alone can fully explain the formation of sedimentary basins.

Models for extensional basin formation based on kinematic thinning are frequently applied to reconstruct particular observed basin stratigraphies and to estimate the basin's thermal history, which is essential for evaluating petroleum prospects. The thermal history is strongly controlled by the value of the thinning factors used to generate the observed basin subsidence. Our results indicate that models with and without mineral phase transitions will provide significantly different thinning factors to generate the same amount of syn-rift or post-rift subsidence. Therefore, thermal histories provided by models with and without mineral phase transitions are likely to be considerably different. Reliable thermal history reconstructions should, therefore, compare the thermal histories obtained by models with and without mineral phase transitions.

Acknowledgements

We thank the Swiss National Fond, project number 21-61912.00, for financial support. YYP and SMS were supported by a Center of Excellence grant to PGP from the Norwegian research council. We thank Taras Gerya, Ed Ghent and Sierd Cloetingh for the reviews of the manuscript, and B. Wood for the editorial comments.

Appendix A. Simplified phase diagrams

Simplified phase diagrams have been derived from the real phase diagrams by least-squares fitting. For this purpose, the mantle phase diagram has been divided into three parts: spinel–lherzolite, plagioclase–lherzolite and garnet–lherzolite. The crustal phase diagram has been divided into two parts, and equations are given in Table A1. The mantle phase diagram has been divided into three parts (Table A2). The maximum error in density is around 1% for mantle compositions and around 6% for crustal compositions. The parameterized phase diagram is valid for the temperatures and pressures that are indicated. The density of rocks at lower temperatures than 200 °C is assumed to be the density at a temperature of 200 °C, since metamorphic reactions become too slow and our equilibrium phase diagram is no longer applicable.

References

[1] D. McKenzie, Some remarks on the development of sedimentary basins, Earth Planet. Sci. Lett. 40 (1978) 25–32.
[2] P.A. Ziegler, N. Cloetingh, Dynamic processes controlling evolution of rifted basins, Earth-Sci. Rev. 64 (2004) 1–50.
[3] I. Walker, K. Berry, J. Bruce, L. Bystol, J. Snow, Structural modelling of regional depth profiles in the Vøring Basin: implications for the structural and stratigraphic development of the Norwegian passive margin, J. Geol. Soc. 154 (1997) 537–544.
[4] L. Royden, C. Keen, Rifting process and thermal evolution of the continental margin of eastern Canada determined from subsidence curves, Earth Planet. Sci. Lett. 51 (1980) 343–361.
[5] C. Beaumont, C. Keen, R. Boutilier, On the evolution of rifted continental margins: comparison of models and observations for the Nova Scotia margin, Geophys. J. R. Astron. Soc. 70 (1982) 667–715.
[6] J.G. Sclater, L. Royden, F. Horvath, B. Burchfield, S. Semken, L. Stegena, The formation of intra-Carpathian basins as determined from subsidence data, Earth Planet. Sci. Lett. 51 (1980) 139–162.
[7] G. Spadini, A. Robinson, S. Cloetingh, Thermo-mechanical modelling of Black Sea formation, subsidence and sedimentation, in: A. Robinson (Ed.), Regional Abd Petroleum Geology of the Black Sea and Surrounding Areas, 1997, pp. 19–38.
[8] S. Ren, J. Faleide, O. Eldholm, J. Skogseid, F. Gradstein, Late Cretaceous–Paleocene tectonic development of the NW vøring basin, Mar. Pet. Geol. 20 (2003) 177–206.
[9] M. Middleton, A model of intracratonic basin formation entailing deep crustal metamorphism, Geophys. J. R. Astron. Soc. 62 (1980) 1–14.
[10] Y. Hamdani, J.C. Mareschal, J. Arkani-Hamed, Phase change and thermal subsidence of the Williston basin, Geophys. J. Int. 116 (1994) 585–597.
[11] Y.Y. Podladchikov, A.N.B. Poliakov, D.A. Yuen, The effect of lithospheric phase-transitions on subsidence of extending continental lithosphere, Earth Planet. Sci. Lett. 124 (1–4) (1994) 95–103.

[12] Y. Hamdani, J.C. Mareschal, J. Arkani-Hamed, Phase changes and thermal subsidence in intracontinental sedimentary basins, Geophys. J. Int. 106 (1991) 657–665.
[13] R.S. Huismans, Y.Y. Podladchikov, S. Cloetingh, Transition from passive to active rifting: relative importance of asthenospheric doming and passive extension of the lithosphere, J. Geophys. Res., [Solid Earth] 106 (B6) (2001) 11271–11291.
[14] E. Burov, A. Poliakov, Erosion and rheology controls on synrift and postrift evolution: verifying old and new ideas using a fully coupled numerical model, J. Geophys. Res., [Solid Earth] 106 (B8) (2001) 16461–16481.
[15] T. Yamasaki, M. Nakada, The effects of the spinel–garnet phase transition on the formation of rifted sedimentary basins, Geophys. J. Int. 130 (1997) 681–692.
[16] R.J. O'Connell, G. Wasserburg, Dynamics of submergence and uplift of a sedimentary basin underlain by a phase change boundary, Rev. Geophys. 10 (1972) 335–368.
[17] E.V. Artyushkov, N.-A. Moerner, D. Tarling, The cause of loss of lithospheric rigidity in areas far from plate tectonic activity, Geophys. J. Int. 143 (2000) 752–775.
[18] J. Lovering, The nature of the Mohorovic discontinuity, Trans.-Am. Geophys. Union 39 (1958) 947–955.
[19] G. Kennedy, The origin of continents, mountain ranges and ocean basins, Am Sci. 97 (1959) 491–504.
[20] H. Neugebauer, T. Spohn, Late stage development of mature Atlantic-type continental margins, Tectonophysics 50 (1978) 275–305.
[21] T. Spohn, H. Neugebauer, Metastable phase transition models and their bearings on the development of Atlantic-type geosynclines, Tectonophysics 50 (1978) 387–412.
[22] K. Petrini, J.A.D. Connolly, Y.Y. Podladchikov, A coupled petrological-tectonic model for sedimentary basin evolution: the influence of metamorphic reactions on basin subsidence, Terra Nova 13 (5) (2001) 354–359.
[23] L.I. Lobkovsky, A. Ismail-Zadeh, B.M. Naimark, A.M. Nikishin, S. Cloetingh, Mechanism of subsidence of the earth crust and sedimentary basin formation (in Russian), Dokl. Akad. Nauk SSSR 330 (2) (1993) 256–260.
[24] L.I. Lobkovsky, S. Cloetingh, A.M. Nikishin, Y. Volozh, A. Lankreijer, A. Belyakov, V. Groshev, P.A. Fokin, E. Milanovsky, L. Pevzner, V.I. Gorbachev, M. Korneev, Extensional basins of the former Soviet Union—structure, basin formation mechanisms and subsidence history, Tectonophysics 266 (1996) 251–285.
[25] J.A.D. Connolly, Multivariable phase-diagrams—an algorithm based on generalized thermodynamics, Am. J. Sci. 290 (6) (1990) 666–718.
[26] J.A.D. Connolly, K. Petrini, An automated strategy for calculation of phase diagram sections and retrieval of rock properties as a function of physical conditions, J. Metamorph. Geol. 20 (7) (2002) 697–708.
[27] S. Taylor, S. McLennan, The Continental Crust: Its Composition and Evolution, Blackwell Scientific Publications, 1985.
[28] K.H. Wedepohl, The composition of the continental crust, Geochim. Cosmochim. Acta 59 (7) (1995) 1217–1232.
[29] A. Ringwood, A model for the upper mantle, J. Geophys. Res. 67 (1962) 857–866.
[30] T. Holland, R. Powell, An internally consistent thermodynamic dataset for phases of petrological interest, J. Metamorph. Geol. 16 (1998) 309–343.
[31] M. Ghiorso, M. Hirschmann, P. Reiners, V. Kress, The pMELTS: a revision of MELTS for improved calculation of phase relations and major element partitioning related to partial melting of the mantle to 3GPa, Geochem. Geophys. Geosyst. 3 (5) (2002), doi:10.1029/2001GC000217.
[32] S.V. Sobo1ev, A.Y. Babeyko, Modeling of mineralogical composition, density and elastic-wave velocities in anhydrous magmatic rocks, Surv. Geophys. 15 (5) (1994) 515–544.
[33] B.J. Wood, D. Yuen, The role of lithospheric phase transitions on seafloor flattening at old ages, Earth Planet. Sci. Lett. 66 (1983) 303–314.
[34] B.J. Wood, J.R. Holloway, A thermodynamic model for subsolidus equilibria in the system CaO–MgO–$A1_2O_3$–SiO_2, Geochim. Cosmochim. Acta 48 (1984) 159–176.
[35] D. Green, T. Falloon, Pyrolite: a ringwood concept and its current expression, in: I. Jackson (Ed.), The Earth's Mantle. Composition, Structure and Evolution, Cambridge University Press, Cambridge, 1998, p. 566.
[36] H. Austrheim, M. Erambert, A. Engvik, Processing of crust in the root of the Caledonian continental collision zone: the role of eclogitization, Tectonophysics 273 (1997) 129153.
[37] J.A.D. Connolly, A.B. Thompson, Fluid and enthalpy production during regional metamorphism, Contrib. Mineral. Petrol. 102 (3) (1989) 347–366.
[38] G. Borse, Numerical methods with MATLAB. A resource for scientists and engineers, PWS Publishing Company, Boston, 1997.
[39] A.M. Rubin, Dikes vs diapirs in viscoelastic rock, Earth Planet. Sci. Lett. 119 (4) (1993) 641–659.
[40] J.A.D. Connolly, Y.Y. Podladchikov, Compaction-driven fluid flow in viscoelastic rock, Geodin. Acta 11 (2–3) (1998) 55–84.
[41] D.C. Rubie, A.B. Thompson, Kinetics of metamorphic reactions at elevated temperatures and pressures, in: A.B. Thompson, D.C. Rubie (Eds.), Metamorphic Reactions: Kinetics, Textures and Deformation, Springer Verlag, New York, 1985, pp. 27–79.
[42] G. Rebay, R. Powell, The formation of eclogite facies metatroctolites and a general petrogenetic grid in Na_2O–CaO–FeO–MgO–$A1_2O_3$–SiO_2–H_2O (NCFMASH), J. Metamorph. Geol. 20 (9) (2002) 813–826.
[43] T.J. Ahrens, G. Schubert, Gabbro-eclogite reaction rate and its geophysical significance, Rev. Geophys. Space Phys. 13 (1975) 383–400.
[44] A.B. Watts, Isostasy and Flexure of the Lithosphere, 1st edition, Cambridge University Press, 2001.
[45] E.B. Burov, M. Diament, The effective elastic thickness (Te) of continental lithosphere: what does it really mean? J. Geophys. Res. 100 (B1) (1995) 3905–3927.
[46] N.J. Kusznir, P.A. Ziegler, The mechanics of continental extension and sedimentary basin formation—a simple-shear

pure-shear flexural cantilever model, Tectonophysics 215 (1–2) (1992) 117–131.
[47] P. Bellingham, N. White, A two-dimensional inverse model for extensional sedimentary basins: 2. Application, J. Geophys. Res., [Solid Earth] 107 (B10) (2002) (art. no.-2260).
[48] H. Kooi, S. Cloetingh, J. Burrus, Lithospheric necking and regional isostasy at extensional basins: 1. Subsidence and gravity modelling with an application to the gulf of lions margin (SE France), J. Geophys. Res. 97 (1992) 17553–17571.
[49] R.T. van Balen, P. van der Beek, S. Cloetingh, The effect of rift shoulder erosion on strata1 patterns at passive margins: implications for sequence stratigraphy, Earth Planet. Sci. Lett. 134 (1995) 527–544.
[50] E. Burov, S. Cloetingh, Erosion and rift dynamics: new thermomechanical aspects of post-rift evolution of extensional basins, Earth Planet. Sci. Lett. 150 (1997) 7–26.
[51] S. Cloetingh, F. Gradstein, H. Kooi, A.C. Grant, M. Kaminsky, Plate reorganisation: a cause of rapid late Neogene subsidence and sedimentation around the North Atlantic? J. Geol. Soc. (Lond.) 147 (1990) 495–506.
[52] H. Kooi, M. Hettema, S. Cloetingh, Lithosphere dynamics and the rapid Pliocene–Quaternary subsidence phase in the southern north sea basin, Tectonophysics 192 (1991) 245–259.
[53] T. Holland, J. Bkaer, R. Powell, Mixing properties and activity-composition relationships of chlorites in the system MgO–FeO–Al_2O_3–SiO_2–H_2O, Eur. J. Mineral. 10 (1998) 395–406.
[54] N. Chatterjee, E. Froese, A thermodynamic study of the pseudo-binary join muscovite–paragonite in the system $KAlSi_3O_8$–$NaAlSi_3O_8$–Al_2O_3–SiO_2–H_2O, Am. Mineral. 60 (1975) 985–993.
[55] R. Newton, T. Charlu, O. Kleppa, Thermochemistry of the high structural state plagioclases, Geochim. Cosmochim. Acta 44 (1980) 933–941.
[56] T. Holland, R. Powell, Thermodynamics of order-disorder in minerals: 2. Symmetric formalism applied to solid solutions, Am. Mineral. 81 (1996) 1425–1437.
[57] Y. Podladchikov, S.M. Schmalholz, D.W. Schmid, Inverse Modelling of Sedimentary Basins, Progress in Industrial Mathematics at ECMI 2000, Springer-Verlag, Berlin, 2002, pp. 625–629.
[58] D.H. Green, W. Hibberson, A. Jaques, Petrogenesis of mid-oceanic ridge basalt, in: M. Mc-Elhinny (Ed.), The Earth: It's Origin, Structure and Evolution, Academic Press, 1979, pp. 265–299.